AIP | Applied Physics Letters

Growth and characterization of van der Waals heterostuctures formed by the topological insulator Bi2Se3 and the trivial insulator SnSe2

A. V. Matetskiy, I. A. Kibirev, A. V. Zotov, and A. A. Saranin

Citation: Applied Physics Letters **109**, 021606 (2016); doi: 10.1063/1.4958936
View online: http://dx.doi.org/10.1063/1.4958936
View Table of Contents: http://scitation.aip.org/content/aip/journal/apl/109/2?ver=pdfcov
Published by the AIP Publishing

Growth and characterization of van der Waals heterostuctures formed by the topological insulator Bi_2Se_3 and the trivial insulator $SnSe_2$

A. V. Matetskiy,[1,2,a)] I. A. Kibirev,[1,2] A. V. Zotov,[1,2,3] and A. A. Saranin[1,2]
[1]*Institute of Automation and Control Processes, Far Eastern Branch of RAS, Vladivostok 690041, Russian Federation*
[2]*Far Eastern Federal University, Vladivostok 690950, Russian Federation*
[3]*Department of Electronics, Vladivostok State University of Economics and Service, Vladivostok 690600, Russian Federation*

(Received 11 May 2016; accepted 5 July 2016; published online 14 July 2016)

The formation, structure and electronic properties of $SnSe_2$–Bi_2Se_3 van der Waals heterostructures were studied. Both heterostructures, $SnSe_2$ on Bi_2Se_3 and Bi_2Se_3 on $SnSe_2$, were grown epitaxially with high crystallinity and sharp interfaces. Their electron band structures are of trivial and topological insulators, respectively. The Dirac surface states of Bi_2Se_3 survive under the $SnSe_2$ overlayer. One triple layer of $SnSe_2$ was found to be an efficient spacer for separating a Bi_2Se_3 topological-insulator slab into two and creating the corresponding topological surface states. *Published by AIP Publishing*. [http://dx.doi.org/10.1063/1.4958936]

Two-dimensional (2D) materials have been one of the most studied topics in solid state physics in the last decade, beginning with graphene[1] followed by numerous other materials. In addition to graphene-like atomic thin sheets, such as hexagonal boron nitride,[2,3] individual layers of the van der Waals crystals, such as transition metal dichalcogenides,[4,5] have been studied.

Layered structures are typical for topological insulators (TIs), which are another exciting topic in the field of condensed matter physics. Similar to graphene, TIs possess metallic Dirac surface states (SSs), which spin–split in addition. These states originate from nontrivial topology and time-reversal symmetry (TRS). They have many potential applications and provide a way to study a variety of fundamental phenomena.[6–8]

The unique material structures of TIs allow artificial materials to be constructed by stacking different 2D crystals on top of each other to obtain the desired properties.[9] Weak van der Waals-like forces are sufficient to hold the stack together, but, in the absence of dangling bonds, the strain between layers is minimal. Here, the concept of van der Waals epitaxy is used.[10] In principle, this enables heteroepitaxy between layered materials with large lattice mismatches.

TI-based heterostructures are characterized by a diverse array of possible phenomena.[11] In heterostructures built with TIs and magnetic insulators, TRS can be broken by the proximity effect,[12–14] which provides a way to observe the topological magnetoelectric effect and quantum anomalous Hall effect.[6] Such heterostructures also provide the possibility of electrostatic control of magnetic anisotropy.[15] Furthermore, a superlattice comprising magnetically doped TIs (another way to break TRS) and trivial insulators provides a simple example of a Weyl semimetal,[16] which is a material that possesses Weyl fermions. In turn, the Majorana fermion can be found in heterostructures based on TIs and superconductors.[17]

The goal of the present study was to grow and characterize van der Waals heterostructures based on the TI Bi_2Se_3 and trivial insulator $SnSe_2$. In particular, with the heterostructures where TI is sandwiched by trivial insulators, one can achieve electrostatic gating across the bulk bandgap of the TI.[18,19] Using superlattices allows for the number of topological SS channels to be multiplied, which drastically increases the surface-to-bulk ratio in transport-related phenomena.[20,21]

Heteroepitaxy of $SnSe_2$ on Bi_2Se_3 (and vice versa) was achieved using molecular beam epitaxy (MBE). Films were smooth, with highly crystalline and sharp interfaces, as revealed by reflection high-energy electron diffraction (RHEED) and scanning tunneling microscopy (STM) observations. Angle-resolved photoemission spectroscopy (ARPES) data showed that, after the $SnSe_2$ film formed on the Bi_2Se_3 layer, the Dirac SSs remain intact. A single $SnSe_2$ triple layer (TL) is sufficient to separate the Bi_2Se_3 stack into two and introduce corresponded topological interface states.

Thin-film growth using MBE was conducted in an ultra-high vacuum (UHV) chamber with base pressure less than 5.0×10^{-10} Torr, equipped with RHEED facility. N-type Si(111) wafers (40–70 $\Omega \cdot$ cm) were used as substrates. An atomically clean Si(111)7×7 surface was prepared *in situ* by flashing to 1280 °C after the wafer was out-gassed at 600 °C for 6 h. Tin, bismuth, and selenium were evaporated from effusion cells with integrated shutters. The prepared samples were transferred into another UHV chamber, equipped with STM, ARPES, and X-ray photoemission spectroscopy (XPS) facilities. The samples were transported without breaking the UHV conditions using an evacuated transfer unit with a base pressure of approximately 1.0×10^{-9} Torr. ARPES and XPS measurements were conducted using a VG Scienta R3000 electron analyzer and high-flux He discharge lamp ($h\nu = 21.2$ eV) and Mg X-ray source ($h\nu = 1253.7$ eV), respectively.

The Bi_2Se_3 film was prepared using a procedure[22] that involved the MBE growth of Bi_2Se_3 on a $\sqrt{3} \times \sqrt{3}$-reconstructed Bi monolayer on Si(111).[23] To grow the $SnSe_2$ film on Bi_2Se_3, we used Se-rich conditions with a Sn to Se ratio of approximately 1:10. The tin deposition rate was approximately 0.25 ML/min (monolayer (ML); 7.8×10^{-14} cm^{-2}),

a)mateckij@iacp.dvo.ru

and the substrate temperature was 190 °C. Reversal scenario of Bi_2Se_3 growth on the $SnSe_2$ was also realized using a growth rate of 0.15 quintuple layer (QL) per minute and a substrate temperature of 190 °C.

Crystal structures of Bi_2Se_3 and $SnSe_2$ are shown in Fig. 1(d). $SnSe_2$ has a CdI_2-type layered structure where each TL consists of one Sn atomic sheet sandwiched between two Se atomic sheets [Fig. 1(d)]. The in-plane lattice constant is $a = 3.8$ Å and the TL-to-TL distance is $h = 6.1$ Å.[24] Bi_2Se_3 layers are arranged in the order Se-Bi-Se-Bi-Se with a QL-to-QL distance of $h = 9.5$ Å and an in-plane lattice constant of $a = 4.14$ Å.

Figures 1(a), 1(b), and 1(c) show RHEED patterns taken along the Si [11$\bar{2}$] direction from the initial Bi_2Se_3 substrate, a 1 TL $SnSe_2$ film, and a 30 TL $SnSe_2$ film, respectively. Ratios of distances between the (00)–(01) spots of the substrate and the film agree well with the reciprocal lattice constants of Bi_2Se_3 and $SnSe_2$. The RHEED pattern from the 1 TL $SnSe_2$ film [Fig. 1(b)] includes faint, streaked spots that are not seen in the RHEED patterns from the Bi_2Se_3 substrate or the 30 TL $SnSe_2$ film. These spots have the highest intensity around the specular spot. The distance between these spots and specular spot coincides with the difference between the (00)–(01) spot distances of the substrate and film. This suggests that these additional spots can be caused by a Moiré pattern with lattice constant $\mathbf{A} = 11 \times \mathbf{a}_{Bi_2Se_3} = 12 \times \mathbf{a}_{SnSe_2} = 45.5$ Å. The Moiré pattern disappears after the second $SnSe_2$ TL forms.

Figure 2 presents STM images of the films. A large-scale STM image of the initial Bi_2Se_3 substrate is shown in Fig. 2(a). The STM profile [Fig. 2(b)] along the red line in Fig. 2(a) shows steps with heights of ≈1 nm, which agrees with the Bi_2Se_3 QL-to-QL distance (0.95 nm). A high-resolution STM

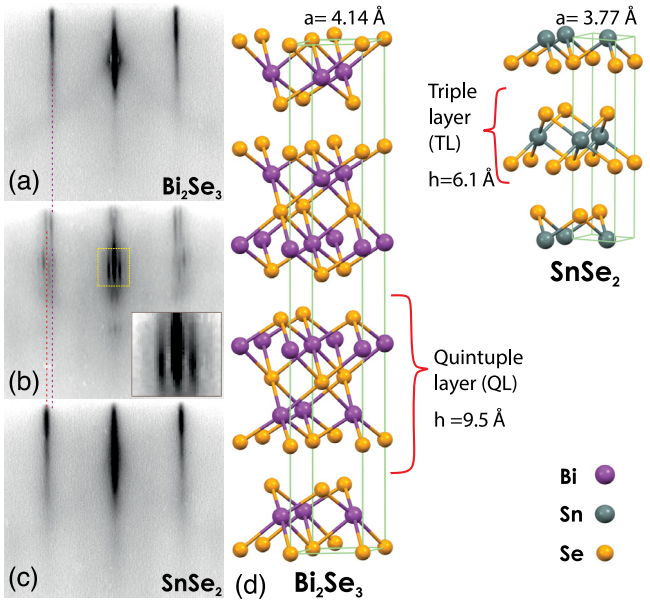

FIG. 1. RHEED patterns from (a) Bi_2Se_3, (b) 1-TL-thick $SnSe_2$ layer grown on Bi_2Se_3, and (c) 30-TL-thick $SnSe_2$ film on Bi_2Se_3. Violet and red dotted lines mark (01) reflections of Bi_2Se_3 substrate and $SnSe_2$ film, respectively. The inset in (b) shows the enlarged region of the RHEED pattern around specular reflection outlined by a yellow dotted rectangle. (d) Ball-and-stick models of Bi_2Se_3 and $SnSe_2$. Bi, Sn, and Se atoms are shown by violet, gray, and yellow balls, respectively. Corresponding bulk unit cells are outlined by green lines.

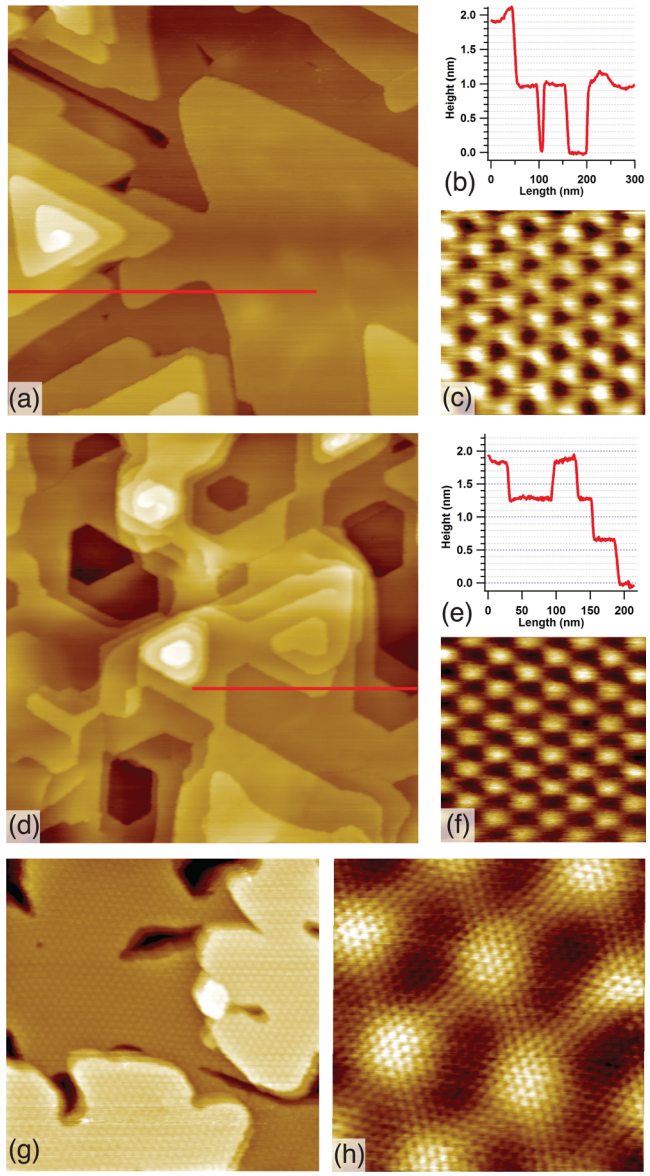

FIG. 2. 400 × 400 nm^2 STM images of (a) 16 QL Bi_2Se_3 on Si(111) and (d) 30 TL $SnSe_2$ on Bi_2Se_3. (b) and (e) STM line profiles along the red lines in (a) and (d), respectively. (c) and (f) 2.5 × 2.5 nm^2 high-resolution STM images of Bi_2Se_3 and 30 TL $SnSe_2/Bi_2Se_3$, respectively. (g) 200 × 200 nm^2 and (h) 12 × 12 nm^2 STM images showing Moiré pattern developing at the surface of the 1-TL-thick $SnSe_2$ layer grown on Bi_2Se_3.

image of the Bi_2Se_3 substrate is shown in Fig. 2(c). A large-scale STM image of the 30-TL-thick $SnSe_2$ film grown on Bi_2Se_3 is shown in Fig. 2(d). The STM profile [Fig. 2(e)] along the red line in Fig. 2(d) shows steps with heights of ≈0.6 nm, which agrees with the $SnSe_2$ TL-to-TL distance (0.61 nm). A high-resolution STM image of the 30-TL-thick $SnSe_2$ film is shown in Fig. 2(f). Except for the occasional screw dislocations, both the substrate and the film are defect-free and atomically smooth, albeit relatively rough over a large scale.

Figures 2(g) and 2(h) present STM images of the 1-TL-thick $SnSe_2$ film grown on Bi_2Se_3. A periodic Moiré pattern with a large lattice constant is visible in Figs. 2(g) and 2(h). Analysis of the high-resolution STM image shown in Fig. 2(h) yields a superlattice periodicity equal to ≈12 interatomic distances, which agrees with estimation derived from the RHEED patterns.

The stoichiometry of the $SnSe_2$ films was proved using XPS. The only peaks present in the XPS spectrum from the 30-TL-thick $SnSe_2$ film [Fig. 3(a)] are from the tin and selenium. The peak–area ratio, normalized using a relative sensitivity factor for Se 3d and Sn 4d, is 1.8:1.0, which is close to the ideal 2:1 stoichiometry.

Experimental ARPES data for $SnSe_2$ have not been reported, and the calculated band structures presented in the literature are not in agreement with each other.[25–27] Our experimental ARPES spectrum for the 30-TL-thick $SnSe_2$ film shown in Fig. 3(b) (presented in the second-derivative mode to enhance fine spectral features) shows a relatively good resemblance with the spectrum calculated for a 1-TL-thick $SnSe_2$ layer.[27] In the experimental spectrum, the valence band maximum is located at the Γ point. Faint spectral features appear near the Fermi level at the M point. This could indicate that the conduction band minimum is approaching the Fermi level; this would suggest that the band gap is indirect and should be close to 1.3 eV.

The fate of topological SS of the Bi_2Se_3 covered by the $SnSe_2$ film was studied. Taking into account that electron escape depth of the excitation energy employed in this study ($h\nu = 21.2$ eV) was approximately 10 Å,[28] we studied only the 1-TL-thick $SnSe_2$ overlayer. The ARPES spectrum around the Γ point for this sample is shown in Fig. 4. The Dirac SS is preserved, and in contrast to the case of magnetic overlayers,[22,29] there are no gap openings at the Dirac point. Additional faint Dirac cone replicas are visible in the ARPES spectrum. Such behavior is typical for films with Moiré patterns. Indeed, the replicas are shifted from the main cone by 0.164 $Å^{-1}$, which coincides with the reciprocal

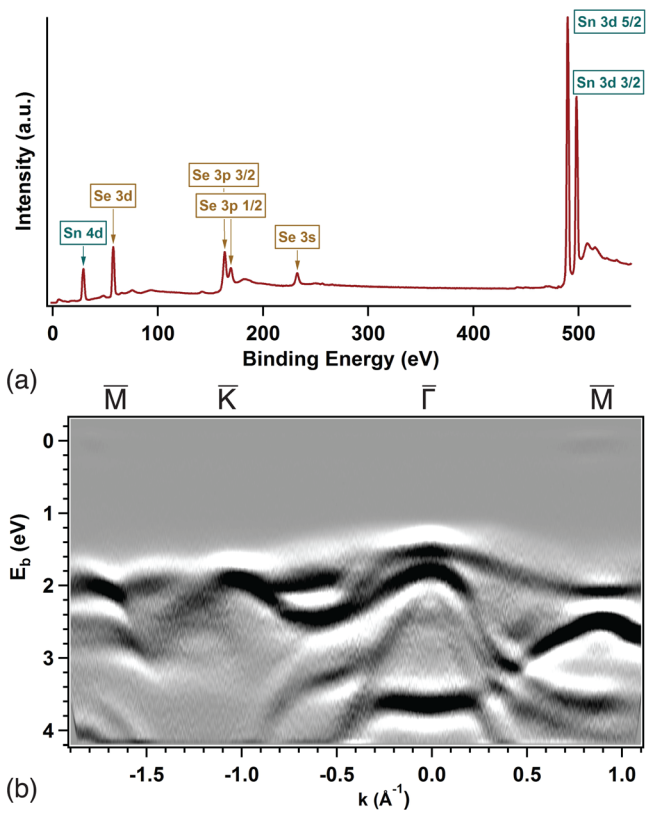

FIG. 3. Spectroscopy data taken from 30-TL-thick $SnSe_2$ film on Bi_2Se_3. (a) XPS spectrum and (b) 2nd-derivative ARPES spectrum.

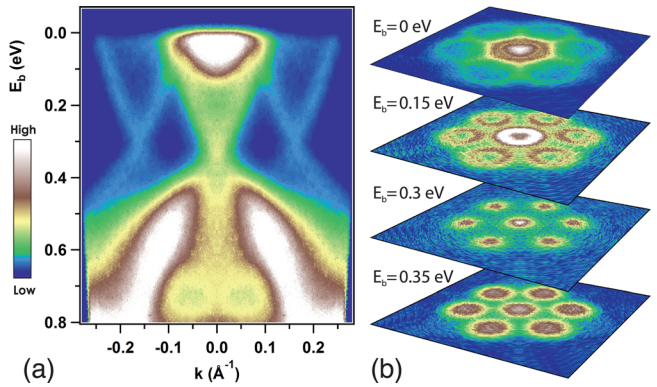

FIG. 4. ARPES data for Bi_2Se_3 covered with 1 TL $SnSe_2$. (a) Symmetrized ARPES spectrum around the Γ point taken at ΓM direction. (b) Constant-energy plots at the Dirac point (≈0.3 eV) and beneath and above it.

lattice constant of the Moiré pattern (0.159 $Å^{-1}$). Replicas can originate from either the final-state effects[30] or effects of a superperiodic potential.[31,32] In general, the latter reflects intrinsic peculiarities of the electronic structure, while the former is associated with the peculiarities of the photoemission process (e.g., electron scattering) in a given system. A superperiodic potential should lead to minigaps appearing at the crossing points of the replicas and in the vicinity of the Bragg planes.[31–33] In the present case, no signs of such features are seen. Thus, we conclude that the replicas most likely originate from the final-state effects, i.e., the wave-vector of the photoelectron ejected from Bi_2Se_3 adopted a reciprocal vector of the Moiré superlattice when the electron passes the $SnSe_2$ layer.

Finally, we examined the possibility of growing the reverse heterostructures, i.e., Bi_2Se_3 on $SnSe_2$. The growth of a Bi_2Se_3 film on a 1-TL-thick $SnSe_2$ layer on Bi_2Se_3 is of interest because in this system, the effect of an ultra-thin trivial insulator spacer on TI stack could be studied. The growth rate was 0.15 QL/min and the substrate temperature was 190 °C. Under these conditions, oscillations of the RHEED specular spot were observed; such oscillations are a sign of layer-by-layer growth. The film has the same basic structure and morphology as the Bi_2Se_3 films grown directly on Si(111). ARPES measurements were used to distinguish the effects of the underlying Bi_2Se_3 on the topological SS of the grown Bi_2Se_3 film through the 1-TL-thick $SnSe_2$ spacer. Figure 5 shows a series of ARPES spectra taken from Bi_2Se_3 films with thicknesses between 2 and 8 QL on a $SnSe_2$ spacer. The 2-QL spectrum [Fig. 5(a)] exhibits two bands separated by a distinct gap. As the film thickness increases to 4 and 6 QL [Figs. 5(b) and 5(c)], the gap gradually decreases and disappears completely at 8 QL [Fig. 5(d)]. The thickness dependence of the topological SS was similar to that of Bi_2Se_3 films grown on graphene.[34] However, in the present case, the hybridization gap closes at larger thicknesses (approximately 8 QL compared with 6 QL[34]), which can be explained by the presence of the additional Bi_2Se_3 surface.

In conclusion, we examined the possibility of growing van der Waals heterostructures from the TI Bi_2Se_3 and the trivial insulator $SnSe_2$. Smooth, epitaxial $SnSe_2$ films with thicknesses from 1 to 30 TL were grown on Bi_2Se_3. Thick SnSe2 films exhibit insulating properties, with an indirect

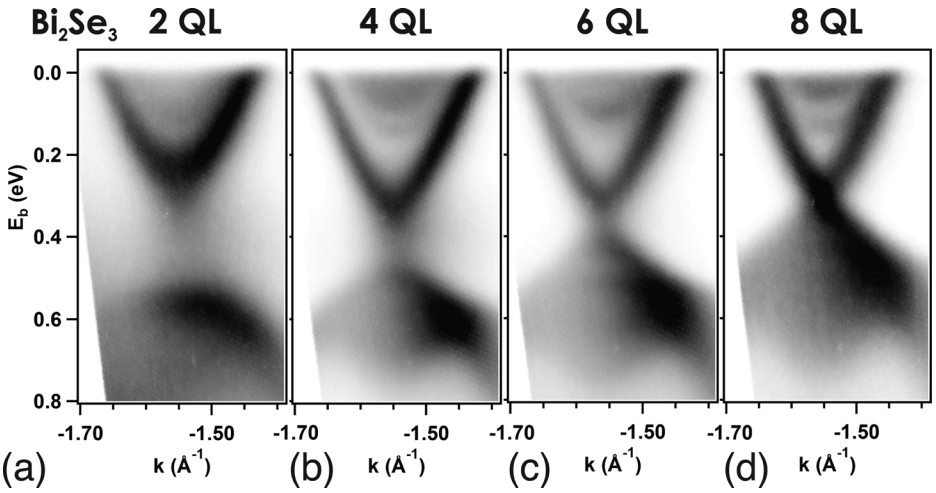

FIG. 5. ARPES spectra around the Γ_1 point taken from (a) 2 QL, (b) 4 QL, (c) 6 QL, and (d) 8 QL Bi_2Se_3 grown on 1-TL-thick $SnSe_2$ spacer on Bi_2Se_3.

gap of 1.3 eV. The 1-TL-thick $SnSe_2$ film grown on Bi_2Se_3 exhibits a Moiré pattern with 12×12 periodicity in units of the $SnSe_2$ lattice constant. This Moiré pattern leads to the appearance of Dirac cone replicas in the ARPES spectra; in the rest, the topological SS remains intact. The 1-TL-thick $SnSe_2$ spacer completely separates the underlying Bi_2Se_3 from the Bi_2Se_3 overlayer, as revealed by the thickness-dependent hybridization gap opening. The Bi_2Se_3–$SnSe_2$ heterostructures could be used in TI-based spintronic devices[11] and new topologically non-trivial materials.[16]

The present work was supported in part by the Grant No. MK-5560.2016.2 of the President of the Russian Federation and the Grant No. 16-02-00505 of the Russian Foundation for Basic Research.

[1]K. S. Novoselov, A. K. Geim, S. V. Morozov, D. Jiang, M. I. Katsnelson, I. V. Grigorieva, S. V. Dubonos, and A. A. Firsov, Nature **438**, 197 (2005).
[2]M. Corso, W. Auwärter, M. Muntwiler, A. Tamai, T. Greber, and J. Osterwalder, Science **303**, 217 (2004).
[3]H. Sediri, D. Pierucci, M. Hajlaoui, H. Henck, G. Patriarche, Y. J. Dappe, S. Yuan, B. Toury, R. Belkhou, M. G. Silly, F. Sirotti, M. Boutchich, and A. Ouerghi, Sci. Rep. **5**, 16465 (2015).
[4]K. F. Mak, C. Lee, J. Hone, J. Shan, and T. F. Heinz, Phys. Rev. Lett. **105**, 136805 (2010).
[5]J. A. Miwa, S. Ulstrup, S. G. Sørensen, M. Dendzik, A. G. Čabo, M. Bianchi, J. V. Lauritsen, and P. Hofmann, Phys. Rev. Lett. **114**, 046802 (2015).
[6]M. Z. Hasan and C. L. Kane, Rev. Mod. Phys. **82**, 3045 (2010).
[7]Y. Ando, J. Phys. Soc. Jpn. **82**, 102001 (2013).
[8]X. L. Qi and S. C. Zhang, Rev. Mod. Phys. **83**, 1057 (2011).
[9]A. K. Geim and I. V. Grigorieva, Nature **499**, 419 (2013).
[10]A. Koma and K. Yoshimura, Surf. Sci. Lett. **174**, A459 (1986).
[11]Y. Guo, Z. Liu, and H. Peng, Small **11**, 3290 (2015).
[12]S. V. Eremeev, V. N. Men'shov, V. V. Tugushev, P. M. Echenique, and E. V. Chulkov, Phys. Rev. B **88**, 144430 (2013).
[13]W. Luo and X.-L. Qi, Phys. Rev. B **87**, 085431 (2013).
[14]P. Wei, F. Katmis, B. A. Assaf, H. Steinberg, P. Jarillo-Herrero, D. Heiman, and J. S. Moodera, Phys. Rev. Lett. **110**, 186807 (2013).
[15]Y. G. Semenov, X. Duan, and K. W. Kim, Phys. Rev. B **86**, 161406(R) (2012).
[16]A. A. Burkov and L. Balents, Phys. Rev. Lett. **107**, 127205 (2011).
[17]L. Fu and C. L. Kane, Phys. Rev. Lett. **100**, 096407 (2008).
[18]D. Kong, Y. Chen, J. J. Cha, Q. Zhang, J. G. Analytis, K. Lai, Z. Liu, S. S. Hong, K. J. Koski, S.-K. Mo, Z. Hussain, I. R. Fisher, Z.-X. Shen, and Y. Cui, Nat. Nanotechnol. **6**, 705 (2011).
[19]H. Steinberg, D. R. Gardner, Y. S. Lee, and P. Jarillo-Herrero, Nano Lett. **10**, 5032 (2010).
[20]J. H. Song, H. Jin, and A. J. Freeman, Phys. Rev. Lett. **105**, 096403 (2010).
[21]Z. Chen, L. Zhao, K. Park, T. A. Garcia, M. C. Tamargo, and L. Krusin-Elbaum, Nano Lett. **15**, 6365 (2015).
[22]A. V. Matetskiy, I. A. Kibirev, T. Hirahara, S. Hasegawa, A. V. Zotov, and A. A. Saranin, Appl. Phys. Lett. **107**, 091604 (2015).
[23]R. H. Miwa, T. M. Schmidt, and G. P. Srivastava, J. Phys.: Condens. Matter **15**, 2441 (2003).
[24]A. Ibarz, E. Ruiz, and S. Alvarez, Chem. Mater. **10**, 3422 (1998).
[25]X. He and H. Shen, Phys. B: Condens. Matter **407**, 1146 (2012).
[26]Y. Huang, C. Ling, H. Liu, S. Wang, and B. Geng, J. Phys. Chem. C **118**, 9251 (2014).
[27]S. Wen, H. Pan, and Y. Zheng, J. Mater. Chem. C **3**, 3714 (2015).
[28]S. Hufner, *Photoelectron Spectroscopy* (Springer, Berlin, Heidelberg, 1996).
[29]Q. Liu, C.-X. Liu, C. Xu, X.-L. Qi, and S.-C. Zhang, Phys. Rev. Lett. **102**, 156603 (2009).
[30]A. Bostwick, T. Ohta, J. L. McChesney, K. V. Emtsev, T. Seyller, K. Horn, and E. Rotenberg, New J. Phys. **9**, 385 (2007).
[31]I. Pletikosić, M. Kralj, P. Pervan, R. Brako, J. Coraux, A. T. N'Diaye, C. Busse, and T. Michely, Phys. Rev. Lett. **102**, 056808 (2009).
[32]P. Moras, P. M. Sheverdyaeva, C. Carbone, D. Topwal, L. Ferrari, G. Bihlmayer, S. Ouazi, S. Rusponi, A. Lehnert, and H. Brune, J. Phys.: Condens. Matter **24**, 335502 (2012).
[33]T. Ohta, J. T. Robinson, P. J. Feibelman, A. Bostwick, E. Rotenberg, and T. E. Beechem, Phys. Rev. Lett. **109**, 186807 (2012).
[34]K. He, Y. Zhang, C.-Z. Chang, C.-L. Song, L.-L. Wang, X. Chen, J.-F. Jia, Z. Fang, X. Dai, W.-Y. Shan, S.-Q. Shen, Q. Niu, X.-L. Qi, S.-C. Zhang, X.-C. Ma, and Q.-K. Xue, Nat. Phys. **6**, 584 (2010).